Evolutionary Models of Convergent Margins : Origin of Their Diversity

Chapter 4

Inconsistent Structure and Motion of the Eastern Median Tectonic Line, Southwest Japan, during the Quaternary

Shigekazu Kusumoto, Keiji Takemura and Yasuto Itoh

Additional information is available at the end of the chapter

http://dx.doi.org/10.5772/67964

Abstract

The Median Tectonic Line (MTL) is the largest tectonic line in southwest Japan, and its eastern portion has moved as a right-lateral fault with a reverse fault component during the Quaternary. Although a high dip of the MTL has been suggested from geomorphological studies, reflection surveys have indicated a low dip of 30–55°. Thus, the MTL shows contradiction between its fault dip and fault motion. In this study, we attempted to re-estimate the dip of the MTL by gravity anomaly, gravity gradient tensor, and numerical simulation, restoring topographies caused by lateral faulting. The numerical simulations suggested that a fault dip of 70–75° is a reasonable dip of the MTL. These high-dip faults are able to move as a lateral fault and have the possibility of reverse fault motion. Deformation patterns caused by faults with these dips are in harmony with the accumulated geological and geomorphological evidence for motions of the MTL. On the other hand, gravity and gravity gradient analyses showed only a material boundary with low dip. This suggested that the MTL does not have conspicuous density contrast at the boundary.

Keywords: motion boundary, material boundary, geophysical prospecting, numerical simulation, fault dip, Median Tectonic Line, Quaternary, lateral fault, reverse fault

1. Introduction

As is well known, the oblique subduction of a plate forms a strike-slip fault parallel to the trench on the continental plate side (e.g., [1]). In general, a fault of this type has vertical or subvertical dip, and these faults have been found widely at plate boundary margins of the world

(e.g., [1, 2]). The Median Tectonic Line (MTL) is a lateral fault located in the plate boundary margin between the Philippine Sea plate and the Eurasian plate (**Figure 1**), and the MTL fits perfectly the class of fault mentioned above.

The MTL, which has a length of more than 1000 km, is the largest tectonic line in southwest Japan, and its eastern portion has moved as a right-lateral fault with a reverse-fault component during the Quaternary. Because the MTL is a very important tectonic line for understanding the tectonics in and around southwest Japan, many geological, geophysical, and geomorphological surveys have been conducted.

Geomorphological studies have suggested that the MTL is basically vertical (e.g., [3, 4]), and its slip rate has been estimated as 5–10 mm/yr in the Shikoku District (e.g., [4]). On the other hand, reflection surveys have indicated a dip of the MTL of between 30 and 55°N (e.g., [5–11]), although Itoh et al. [12] found high-dip faults in the Quaternary layer. In general, it is known that such low-dip faults could not move as a lateral fault, because the overburden pressure acting on the fault plane would be too large to allow lateral motion and the dips would not have optimum orientation for releasing the shear stress (e.g., [13, 14]). In order to solve this inconsistency, Sato et al. [15] suggested that the MTL, which functioned as a megathrust in the Cretaceous, was reactivated as a strike-slip fault under subsequent-phase shear stresses.

In addition to these scientific interests, there are some societal concerns or desires pertaining to this tectonic line. As mentioned above, the MTL, with a length of more than 1000 km, is the

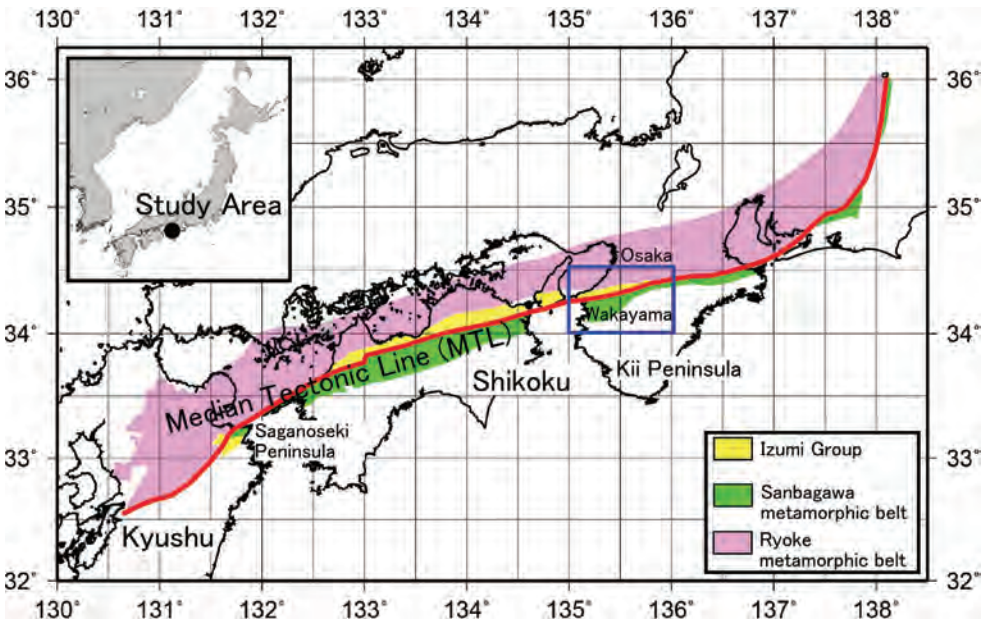

Figure 1. Location map of study area and simplified geological map (based on Hayama and Yamada [67]). Red line is the Median Tectonic Line (MTL). Blue rectangle indicates the study area.

http://dx.doi.org/10.5772/67964

largest tectonic line in southwest Japan. Consequently, several cities are in proximity to the MTL. In particular, there are large cities and international airports around the eastern end of its Quaternary activity.

The dip of a fault affects the size of its area of disaster occurrence (e.g., [16, 17]) and is an important parameter in numerical simulations for hazard map development (e.g., [18]). In general, the size of the area of disaster occurrence is wider on the hanging wall side than on the footwall side of a fault (e.g., [17]). Consequently, if the MTL was a low-dip fault, as shown in reflection surveys, and were to move, the Osaka area at the Kii Peninsula (the eastern end of Quaternary MTL activity) would sustain serious damage. On the other hand, if the MTL was a high-dip fault, as suggested by geomorphological studies, and were to move, both the Osaka area and the Wakayama area of the Kii Peninsula would sustain damage. Therefore, knowing the dip of the MTL, as a seismogenic fault, is very important not only for advancing scientific knowledge but also for societal reasons.

In this study, we attempted to estimate the dip of the MTL from the viewpoints of both a material boundary and a motion boundary. For estimation of the MTL fault dip as a material boundary, we employed gravity anomaly and gravity gradient tensor data, as excellent seismic surveys have been conducted on the MTL. For estimation of the MTL fault dip as a motion boundary, we employed numerical simulations based on dislocation theory in an elastic medium and evaluated deformation fields at the fault terminus caused by lateral fault motions.

2. The gravity anomaly and its interpretations

In this study, we used the Bouguer anomaly database of Komazawa [19]. As the Bouguer anomaly database employed here provides users with 0.5 km × 0.5 km mesh data, we could discuss structures with sizes larger than several kilometers.

Figure 2 is the residual Bouguer anomaly map of the study area. Here, we employed the Bouguer anomaly data of which the Bouguer density is 2670 kg/m^3. In order to obtain the residual Bouguer anomaly map, we estimated the first trend surface of the Bouguer anomaly in this region by the least-squares method from the Bouguer anomaly and removed it from the original Bouguer anomaly data.

Figure 2 is characterized by a distribution of gravity lows and highs. The gravity lows occur in the Izumi Mountains and on the Wakayama Plain and the gravity highs are distributed on the north and south sides of these gravity lows. By comparing **Figure 2** with **Figure 3** (the surface geological map), we found that the gravity highs correspond to outcrops of the Sanbagawa metamorphic rocks and the Ryoke plutonic rocks. The gravity lows are observed in the Izumi Mountains, consisting of gravel, sandstone, and mudstone of the late Cretaceous, and in the Wakayama Plain, consisting of Quaternary sediments, because the densities of these lithologies are not high.

As is well known, techniques for extracting the locations of structural boundaries (namely, edge), without geological and geophysical information, from a gravity anomaly map are called

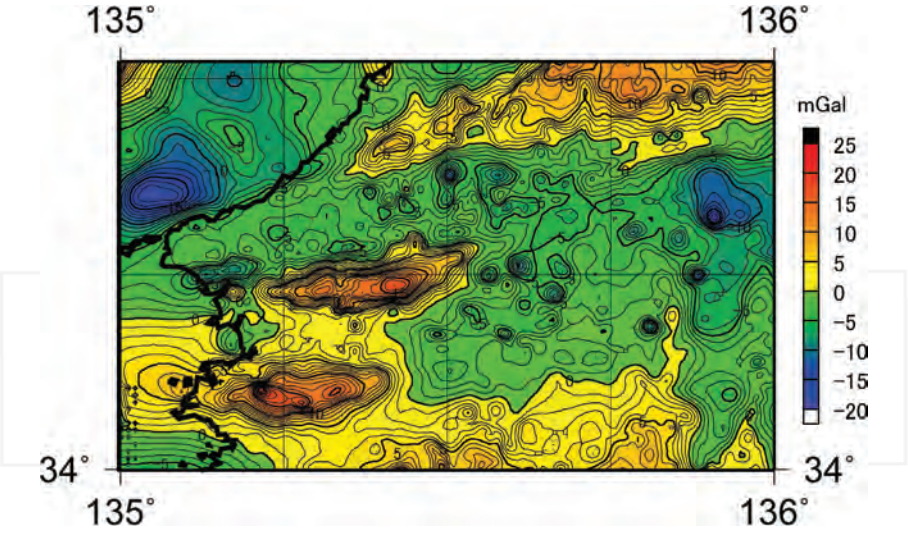

Figure 2. Residual Bouguer anomaly map of the study area and surroundings. The contour interval is 1 mGal. In the residual Bouguer anomaly map, the regional linear trend of the Bouguer anomalies, such as the effect of the subducting plate, is estimated and removed by the least-squares method from the Bouguer anomalies. The Bouguer anomaly used here is based on the gravity anomaly database (0.5 km × 0.5 km mesh data) by Komazawa [19], and a Bouguer density of 2670 kg/m^3 is employed.

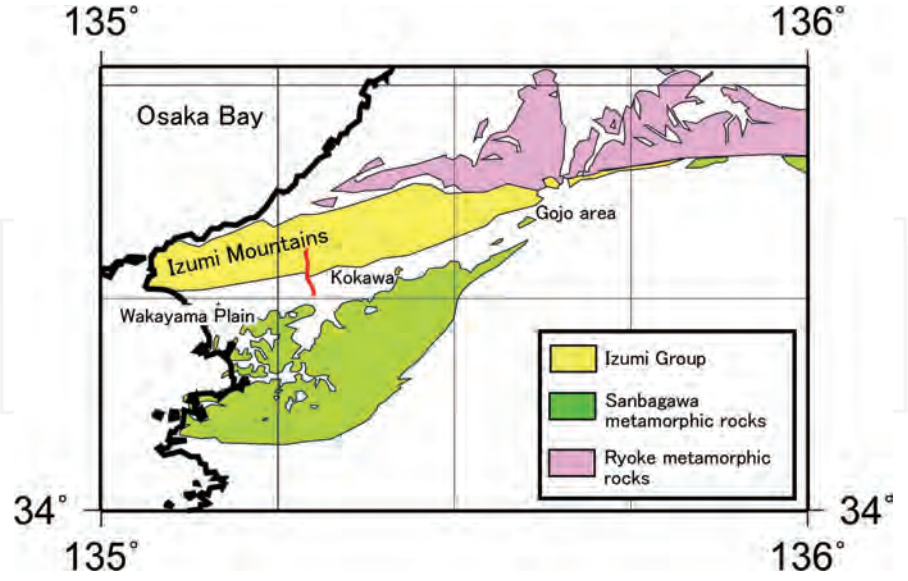

Figure 3. Simplified geological map of the study area (based on Ref. [68]). Izumi Group, Ryoke metamorphic rocks (granites and plutonic rocks), and Sanbagawa metamorphic rocks are shown. The red line in this figure indicates the seismic survey line shown in **Figure 8**.

http://dx.doi.org/10.5772/67964

semi-automatic interpretation methods. These techniques have played an important role in the qualitative interpretation of gravity anomaly maps. A typical technique is the horizontal gravity gradient method (e.g., [20, 21]), which uses the horizontal gravity gradient *HG* defined as follows:

$$HG = \sqrt{\left(\frac{\partial g}{\partial x}\right)^2 + \left(\frac{\partial g}{\partial y}\right)^2}, \tag{1}$$

where g is the Bouguer anomaly. The horizontal gravity gradient method has frequently been employed to find edges caused by structural boundaries such as faults or material boundaries (e.g., [22–24]).

In recent years, more sensitive and keen methods have been developed, and their extraction abilities have been investigated (e.g., [25, 26]). Li et al. [25] evaluated the extraction abilities of existing semi-automatic interpretation methods by numerical tests and pointed out following characteristics. The *HG* method (e.g., [20]), shown by Eq. (1) can determine structural boundaries of the causative body but has decreased ability with depth. The *TDR* (Eq. (2); [27]),

$$TDR = \arctan\left[\frac{\frac{\partial g}{\partial z}}{\sqrt{\left(\frac{\partial g}{\partial x}\right)^2 + \left(\frac{\partial g}{\partial y}\right)^2}}\right], \tag{2}$$

and the *THETA* (Eq. (3); [28]),

$$THETA = \arccos\left[\frac{\sqrt{\left(\frac{\partial g}{\partial x}\right)^2 + \left(\frac{\partial g}{\partial y}\right)^2}}{\sqrt{\left(\frac{\partial g}{\partial x}\right)^2 + \left(\frac{\partial g}{\partial y}\right)^2 + \left(\frac{\partial g}{\partial z}\right)^2}}\right], \tag{3}$$

are also able to extract edges, but these methods draw a phantom edge at the zero line in the case of side-by-side positive and negative anomalies. The *TDX* (Eq. (4); [29])

$$TDX = \arctan\left[\frac{\sqrt{\left(\frac{\partial g}{\partial x}\right)^2 + \left(\frac{\partial g}{\partial y}\right)^2}}{\left|\frac{\partial g}{\partial z}\right|}\right], \tag{4}$$

has the same phantom edge but can provide a clearer edge than the *TDR* or *THETA*.

Zhang et al. [26] showed that the *ILP* (Eq. (5); [30]),

$$ILP = \arcsin\left[\frac{\sqrt{\left(\frac{\partial g}{\partial x}\right)^2 + \left(\frac{\partial g}{\partial y}\right)^2}}{\sqrt{\left(\frac{\partial g}{\partial x}\right)^2 + \left(\frac{\partial g}{\partial y}\right)^2 + \left(\frac{\partial^2 g}{\partial x^2} + \frac{\partial^2 g}{\partial y^2}\right)^2}}\right], \tag{5}$$

and the *TAHG* (Eq. (6); [31]),

$$TAHG = \arctan\left[\frac{\frac{\partial HG}{\partial z}}{\sqrt{\left(\frac{\partial HG}{\partial x}\right)^2 + \left(\frac{\partial HG}{\partial y}\right)^2}}\right], \tag{6}$$

successfully extract the edges of potential field data relating to multisubsurface structures. For evaluating extraction ability, Li et al. [25] and Zhang et al. [26] employed the cube model and the rectangular parallelepiped model, which have vertical structural boundaries.

To extract the edge of the MTL trace from the residual Bouguer anomaly data shown in **Figure 2**, we applied the *HG*, *TDX*, *ILP*, and *TAHG*, which have been confirmed as excellent extraction methods. **Figures 4–7** show the results obtained by each method.

The *HG* method successfully extracted high-gradient anomalies between gravity highs and gravity lows (**Figure 4**). Additionally, the method extracted east-west trending, short, high-gradient anomalies on the Wakayama Plain and the boundary between the plain and the Izumi Mountains. However, these anomalies are not linked to one another continuously, and it is difficult to state that the *HG* method was able to extract the trace of the MTL sufficiently.

The *TDX*, *ILP*, and *TAHG* indicate structural boundary locations by their peak values. Similar to the *HG* method, the *TDX* method successfully extracted high-gradient anomalies between gravity highs and gravity lows (**Figure 5**). Although the method also extracted the east-west trending lines, they do not correspond to the trace of the MTL. The *TDX* at the northern part might indicate boundaries among the Quaternary sediments of the Osaka Plain, the Ryoke plutonic rocks, and the Izumi Group that forms the Izumi Mountains.

The *ILP* and *TAHG* methods were developed to find the edge of the potential fields related to multi subsurface structures, and they generally emphasize very small signals caused by deep structures. The *ILP* map extracted the east-west trending lines, but it is difficult to determine whether or not the map extracted the MTL trace (**Figure 6**). The *TAHG* map is similar to the *ILP* map and has similar difficulties of interpretation (**Figure 7**).

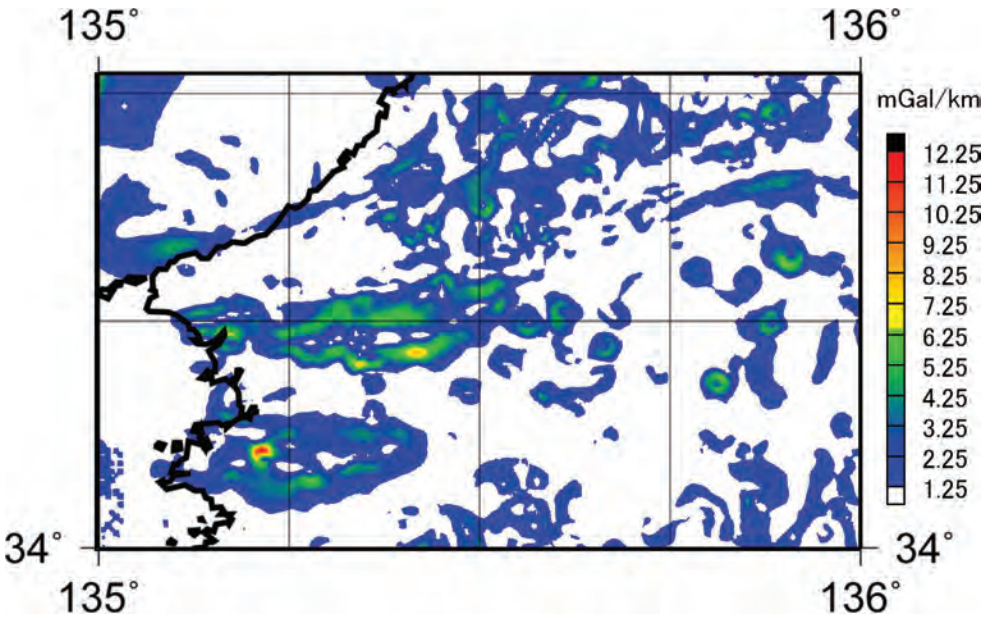

Figure 4. Horizontal gravity gradient map for values over 1.25 mGal/km. Colored areas indicate locations of structural boundaries such as faults or contacts between different materials.

http://dx.doi.org/10.5772/67964

From these results, we can only conclude that these extraction methods cannot extract the MTL trace sufficiently. Thus, we considered that there would be no conspicuous density contrast around the MTL. In the next section, we estimate the density contrast between the Izumi Group and the Quaternary sediments in the Wakayama Plain.

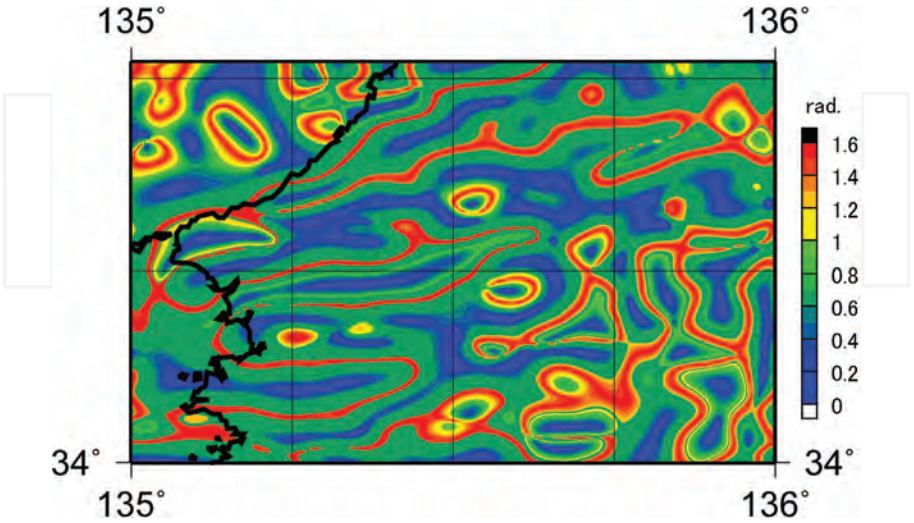

Figure 5. *TDX* map. Units are radians. This map indicates geological or structural boundary by the line *TDX* = max (here, *TDX* = 1.6).

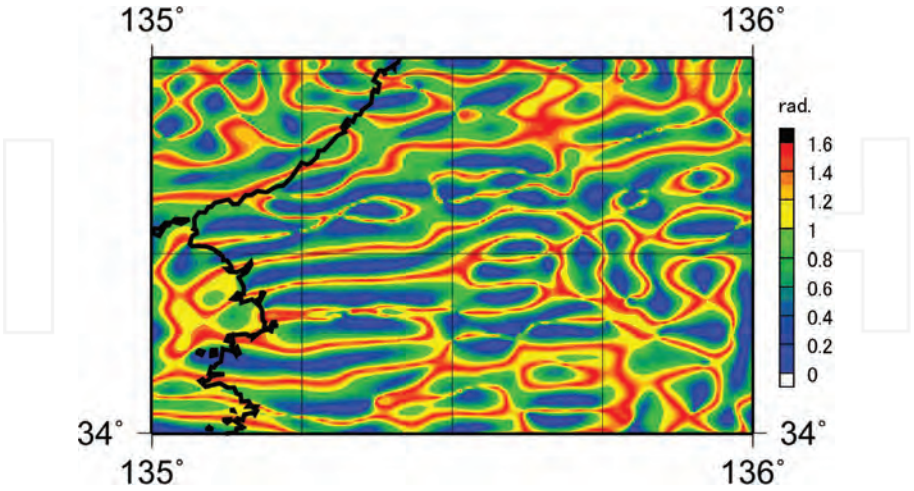

Figure 6. *ILP* map. Units are radians. This map extracts the edge of the gravity anomaly related to multisubsurface structures.

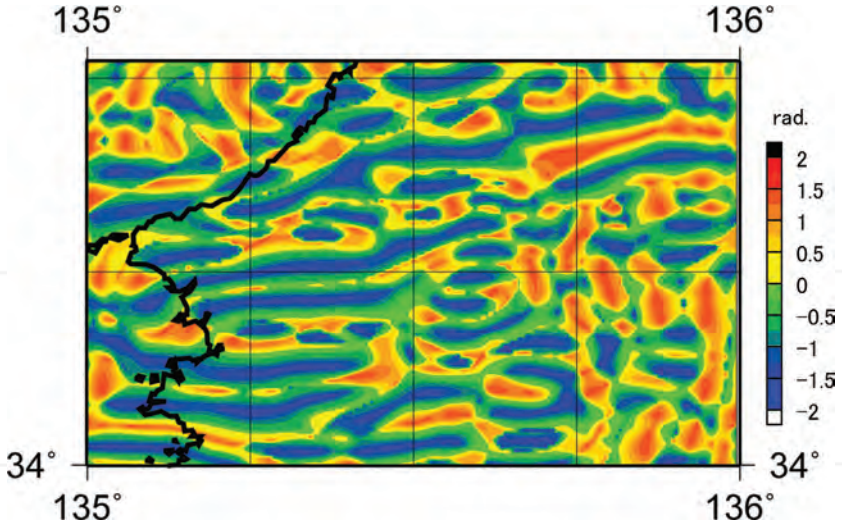

Figure 7. *TAHG* map. Units are radians. This map extracts the edge of the gravity anomaly related to multisubsurface structures.

3. Estimation of density contrast around the MTL

Figure 8 shows a depth-converted seismic profile crossing the MTL (red line shown in **Figure 3**) [32]. Here, the MTL is the boundary between the Izumi Group and the Quaternary sediment. **Figure 8** shows that the dip angle of the MTL is high near the surface but that it becomes gradually lower with depth.

Here, we simplified the subsurface structure (**Figure 8**) to a three-layer model (**Figure 9**), and we assigned densities of 2800 and 2400 kg/m^3 to the lowest layer equivalent to the Sanbagawa metamorphic rocks and the uppermost layer equivalent to the Izumi Group, respectively. The density of the Sanbagawa metamorphic rocks was referred to that at Saganoseki Peninsula, Oita, Kyushu (e.g., [33]). The density of the Izumi Group was a density typical of the solidified sediment. In this study, we changed the density of the Quaternary sediment layer within the range of 2000–2400 kg/m^3 and estimated the optimum density of the Quaternary sediment layer by comparing the calculated Bouguer anomalies with the observed ones. The two-dimensional Talwani's method [34] was employed for the calculations.

The results are summarized in **Figure 10**, and they show that the optimum density of the Quaternary sedimentary layer is 2300 kg/m^3. This supports the subsurface structures estimated by the seismic reflection survey, and it indicates that there is no conspicuous density contrast around the MTL. Specifically, the MTL is a low-dip fault as a material boundary, and its motion boundary is difficult to identify by gravity anomalies because it does not have a conspicuous density contrast.

http://dx.doi.org/10.5772/67964

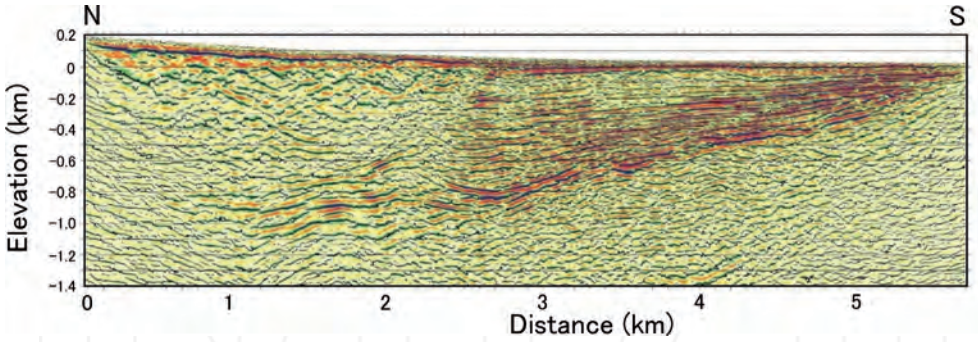

Figure 8. Depth-converted seismic profile crossing the MTL (after Ref. [32]). Location of this profile is shown in **Figure 2** by the red line.

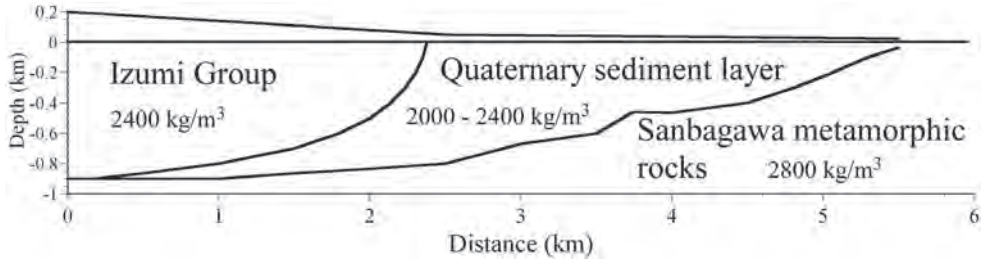

Figure 9. Simplified subsurface structure model based on the depth-converted seismic profile shown in **Figure 8**.

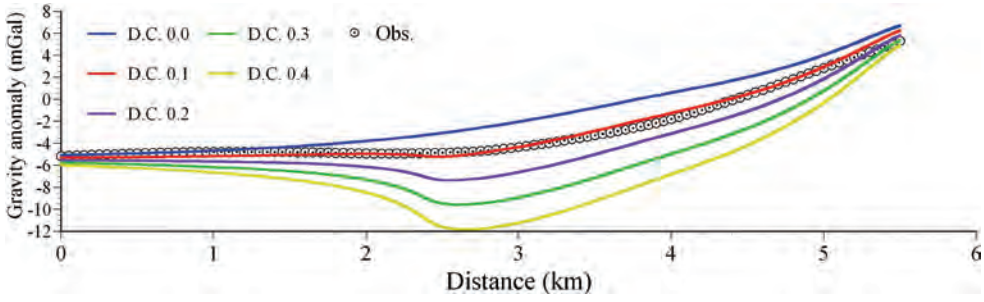

Figure 10. Estimation of the density contrast among the Izumi Group, the Sanbagawa metamorphic rocks, and the Quaternary sediment. In this figure, the circles indicate the observed gravity anomalies, and the colored lines indicate the calculated gravity anomalies from assumed subsurface density structures. Values of D.C. X.X indicate the density contrast between the Izumi Group and the Quaternary sediment in the unit of g/cm^3. For example, D.C. 0.1 means that the density contrast between the Izumi Group and the Quaternary sediment is 0.1 g/cm^3 (=100 kg/m^3).

4. Analysis using the gravity gradient tensor

In recent years, the gravity gradient tensor, whose response to subsurface structures is more sensitive than that of the gravity anomaly, has been employed for obtaining detailed subsurface structure data. The gravity gradient tensor Γ is defined by the differential coefficients of the gravitational potential W (e.g., [35, 36]) as follows:

$$\Gamma = \begin{bmatrix} \frac{\partial^2 W}{\partial x^2} & \frac{\partial^2 W}{\partial y \partial x} & \frac{\partial^2 W}{\partial z \partial x} \\ \frac{\partial^2 W}{\partial x \partial y} & \frac{\partial^2 W}{\partial y^2} & \frac{\partial^2 W}{\partial z \partial y} \\ \frac{\partial^2 W}{\partial x \partial z} & \frac{\partial^2 W}{\partial y \partial z} & \frac{\partial^2 W}{\partial z^2} \end{bmatrix}. \tag{7}$$

The gravity gradient tensor is symmetric (e.g., [35]), and the sum of its diagonal components is zero as the gravitational potential satisfies Laplace's equation:

$$\frac{\partial^2 W}{\partial x^2} + \frac{\partial^2 W}{\partial y^2} + \frac{\partial^2 W}{\partial z^2} = 0. \tag{8}$$

Various analysis techniques using the gravity gradient tensor have been suggested and discussed (e.g., [37–41]). Among these methodologies, Beiki and Pedersen [42] showed that the maximum eigenvector of the gravity gradient tensor points to the causative body (**Figure 11a**). Kusumoto [43] considered that the basement consists of an aggregate of high-density prisms (**Figure 11b**) and applied Beiki's technique [42, 44] to the estimation of the fault dip. This method provided results in which the fault dip estimated by the gravity gradient tensor was in harmony with the dip observed from seismic surveys [43, 45].

Kusumoto [46] showed that in two-dimensional analysis the maximum eigenvector of the tensor points to a high-density causative body (**Figure 11a**) and that the dip of the maximum eigenvector closely follows the dip of the normal fault (**Figure 11b**). In addition, he showed that the minimum eigenvector of the tensor points to a low-density causative body (**Figure 11c**) and that the dip of the minimum eigenvector closely follows the dip of the reverse fault (**Figure 11d**).

In two-dimensional analysis, the gravity gradient tensor Γ_{2D} on the profile is defined as follows (e.g., [38]):

$$\Gamma_{2D} = \begin{bmatrix} \frac{\partial^2 W}{\partial x^2} & \frac{\partial^2 W}{\partial z \partial x} \\ \frac{\partial^2 W}{\partial x \partial z} & \frac{\partial^2 W}{\partial z^2} \end{bmatrix}. \tag{9}$$

Because the gravity potential satisfies the Laplace's equation $\partial^2 W/\partial x^2 + \partial^2 W/\partial z^2 = 0$, we find the relationship $\partial^2 W/\partial z^2 = -\partial^2 W/\partial x^2$. Additionally, $\partial^2 W/\partial x \partial z = \partial^2 W/\partial z \partial x$, because the gravity gradient tensor is a symmetric tensor (e.g., [35]).

As gravity gradiometry surveys have not been conducted in this study area, we estimated the gravity gradient tensor from the gravity anomalies on the seismic reflection survey profile (**Figure 10**), using the Fourier transform method (e.g., [46, 47]), and calculated the dips of the maximum and minimum eigenvectors of the tensor. The dips, α, of the maximum and minimum eigenvectors of the tensor were calculated by

http://dx.doi.org/10.5772/67964

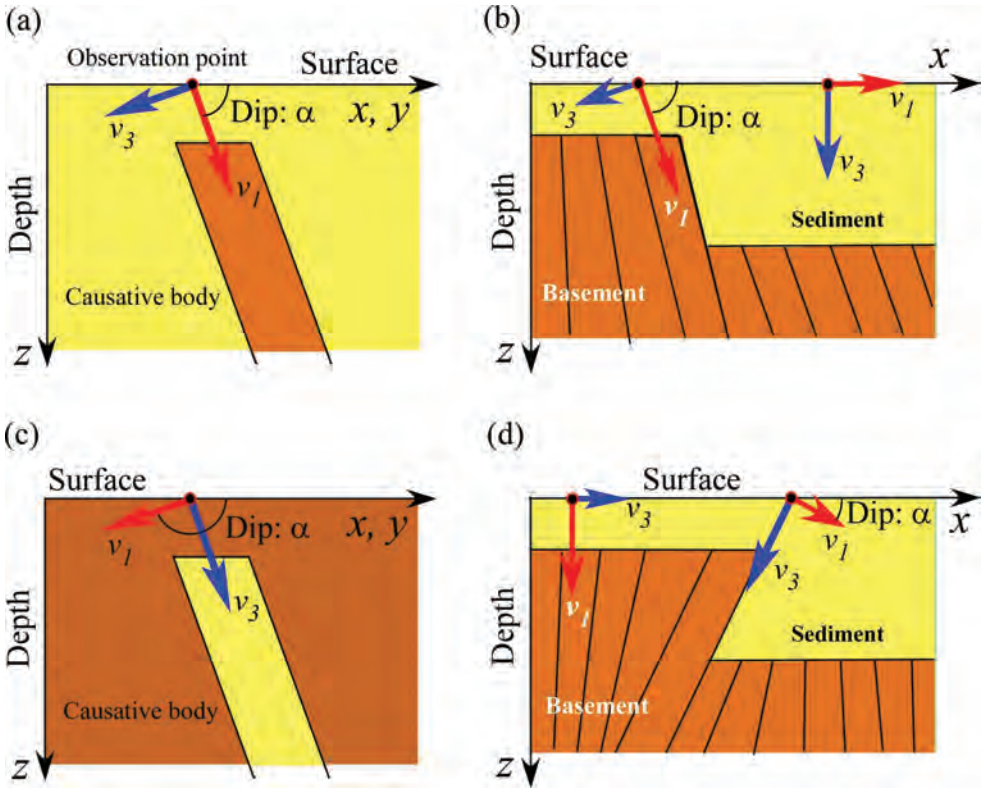

Figure 11. Schematic illustration of the maximum eigenvector and the minimum eigenvector for two-dimensional (2-D) structures. (a) Basic model (high-density causative body model). In this figure, v_1 and v_3 are the maximum eigenvector (red) and the minimum eigenvector (blue) of the gravity gradient tensor, respectively. The maximum eigenvector points to the high-density causative body (brown). (b) Normal fault model. The basement consists of an aggregate of high-density prisms (brown), and the angle, α, of the maximum eigenvector (red) of the tensor follows the fault dip. The minimum eigenvector on the thick sedimentary layer points to the vertical. (c) Low-density causative body model. The minimum eigenvector points to the low-density causative body (light yellow). (d) Reverse fault model. The basement consists of an aggregate of high density prisms (brown), and the angle, α, of the minimum eigenvector (blue) of the tensor follows the fault dip. The maximum eigenvector (red) on the basement points to the vertical.

$$\alpha = \arctan\left(\frac{v_z}{v_x}\right), \tag{10}$$

where v_x and v_z are the x and z components of each eigenvector, respectively.

Figure 12 shows each component of the gravity gradient tensor, and **Figure 13** shows the distributions of the maximum eigenvector (red) and the minimum eigenvector (blue) of the gravity gradient tensor. From **Figure 13**, it was found that the dips of the maximum eigenvectors follow the dip of the Sanbagawa metamorphic layer. On the other hand, the minimum eigenvector points vertically, and the dips of the eigenvectors do not follow the fault dip of the MTL. We considered that this occurs because the structural boundary could not be recognized due to the low-density sediment layers near the surface in the Izumi Group and in

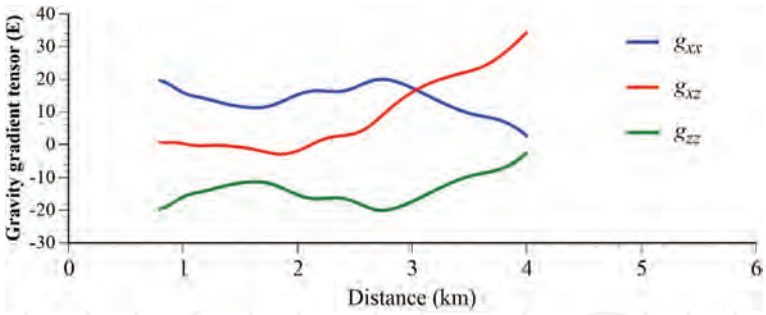

Figure 12. Gravity gradient tensor on the profile. These are estimated from the observed Bouguer anomalies on the profile shown in **Figure 10**.

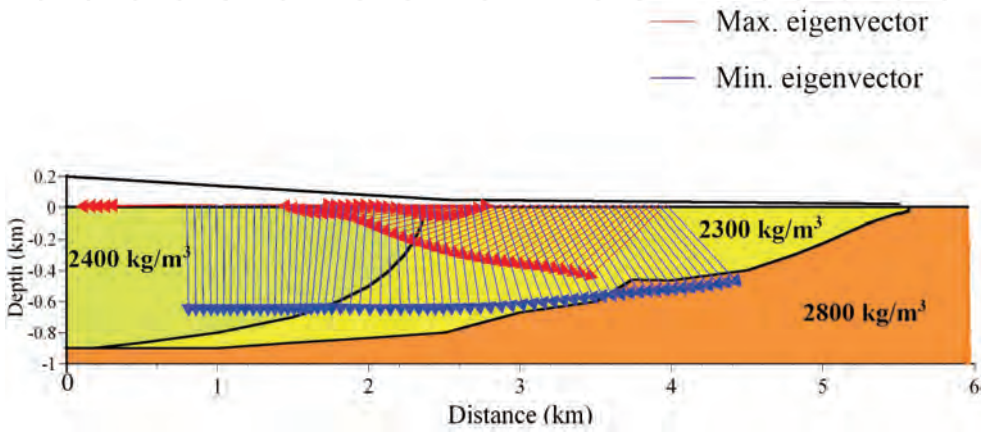

Figure 13. Eigenvectors of the gravity gradient tensor on the profile shown in **Figure 12**. The maximum eigenvector and minimum eigenvector are indicated by red and blue, respectively. The dips of eigenvectors are given clockwise from *x*-axis to *z*-axis.

the Quaternary layer areas. As shown in the previous subsection and in **Figure 10**, there is no conspicuous density contrast. Because the gravity gradient tensor is very sensitive to the subsurface structure near the surface, if a low density layer existed near the surface, the minimum eigenvector of the tensor would point to the low density layer, namely vertically.

5. Surface deformations due to strike-slip fault

The gravity anomaly and gravity gradient tensor cannot recognize or extract the fault location and shape if a conspicuous density contrast does not exist. Dip-slip faults in the thick sedimentary layers and very low-dip faults and lateral faults in the isotropic medium would be examples.

http://dx.doi.org/10.5772/67964

The MTL has both low-dip and lateral fault components. Thus, the gravity anomaly and gravity gradient tensor analyses could not extract the fault trace of the MTL nor estimate the fault dip. The remaining problem is how a low-dip reverse fault could move as a lateral fault: the contradiction between its fault dip and its fault motion.

Thus far, the fault dip and the fault shape have been discussed only as a material boundary because they have been estimated from geophysical explorations such as seismic surveys and gravity surveys. We think that this is the main reason for the contradiction. Using numerical simulations, we thus examined the fault dip of the MTL from the viewpoint of the fault motion, namely, by restoration of the tectonic topography caused by the fault motion.

In the numerical simulations, we employed dislocation modeling, which is often used for quantitative interpretation of crustal deformation caused by earthquakes and/or volcanic activities (e.g., [48–52]). Surface or interior displacements or strains can be calculated by considering dislocations on a plane embedded in an elastic isotropic half-space (**Figure 14**). The dislocation modeling employed here was Okada's dislocation solutions [53] and is defined within a range of the linear elasticity. Consequently, the modeled structures could not be compared directly with the actual geological structures. However, if we simply assume that the geological structures are the accumulation of the deformations caused by the fault motions, dislocation modeling can be a very useful tool because it provides the essential deformation pattern from the minimum number of parameters (fault parameters and elastic constants of the medium).

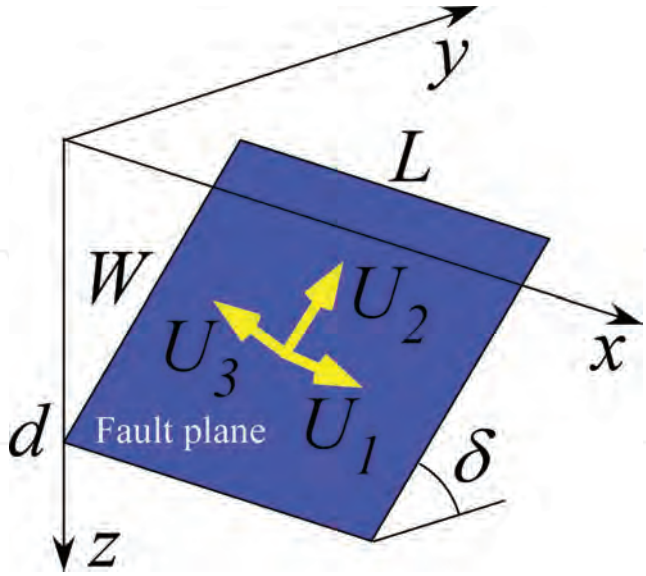

Figure 14. Dislocation plane. *W*, *L*, *d*, and δ are width, length, depth, and dip of the fault. U1, U2, and U3 are strike-slip, dip-slip, and tensile components of arbitrary dislocation. Positive U1 and U2 means left-lateral slip and thrust slip with $0 < \delta < \pi/2$.

In this study, we evaluated how the displacement fields at the terminus of the lateral fault would change if the fault dip was changed. A conspicuous vertical deformation field formed by lateral fault motion occurred at the terminus of the fault, and this did not occur at other areas (**Figure 15**). Geological structures formed by lateral faulting, such as the pull-apart basin, are the result of the accumulation of vertical deformation (subsidence) at the fault terminus area (e.g., [54–56]). In the numerical simulations for restoring these structures, if the geological evidence suggested that the active zone of a lateral fault shifted along its strike direction over time, we expressed its tectonic history by superimposing analytical solutions for different fault lengths (e.g., [57–59]). Hence, we paid attention to the vertical deformation pattern at the fault terminus.

In **Figure 16**, we show predicted vertical deformations at the terminus due to lateral faulting with dips of 45, 60, 70, 75, 80, and 90°. The length and width of the assumed fault model were 30 and 15 km, respectively, and the top of the model was the surface. We set a right-lateral motion of 1 m on the dislocation plane in each model, and a Poisson's ratio of 0.25 was assumed. **Figure 16** shows deformation fields within a distance of 5 km around the fault, and the deformation is the total of both the vertical and the horizontal deformations caused by the right-lateral fault motion. The light-purple thin line in this figure indicates vertical deformation of zero.

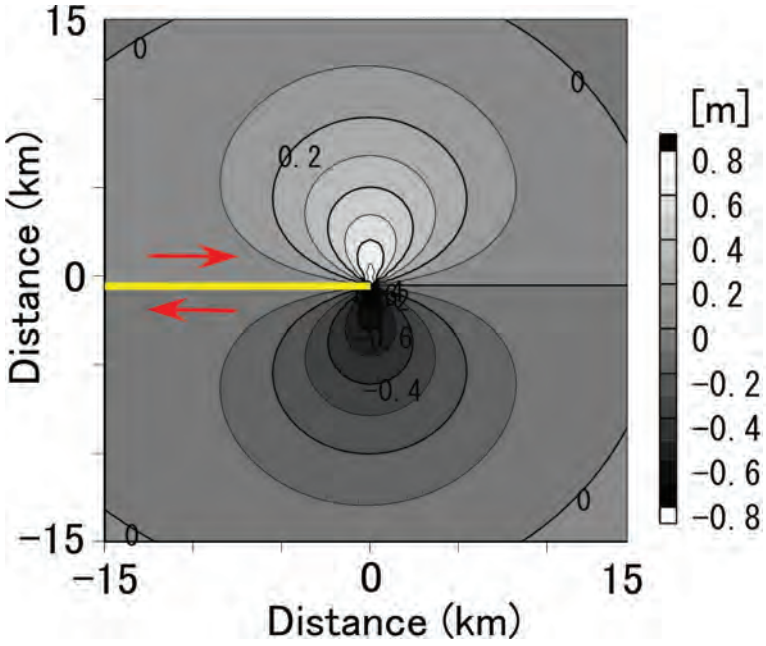

Figure 15. Deformation pattern at the fault terminus caused by right-lateral motion of 1 m. The fault dip is 90°. Yellow line indicates the location of the vertical fault, and red arrows indicate directions of fault motion.

http://dx.doi.org/10.5772/67964

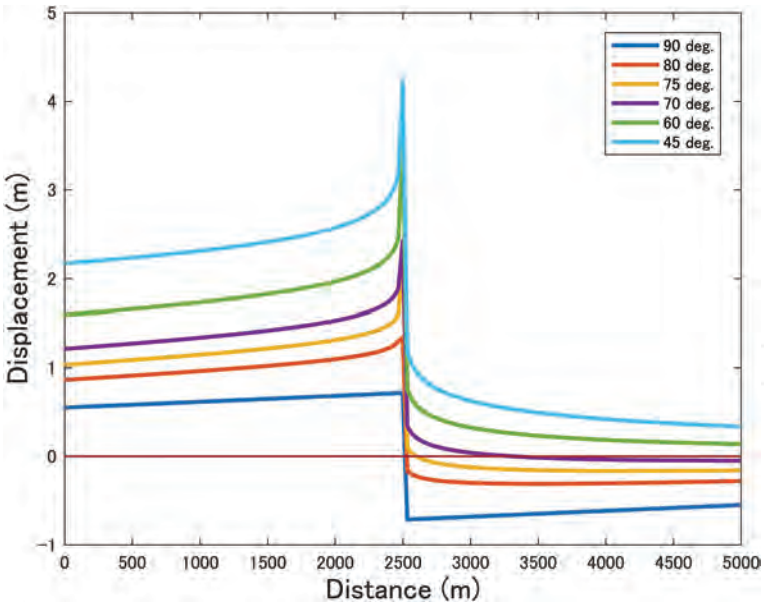

Figure 16. Predicted vertical deformations at the terminus due to lateral faulting with dips of 45, 60, 70, 75, 80, and 90°. The light-purple thin line indicates vertical deformation of zero.

From **Figure 16**, it was found that the basement on the footwall side would not subside if the fault dip is lower than 70°. Specifically, if the fault dip is lower than 70°, the areas around the terminus of the lateral fault would become uplift areas and areas of subsidence would not form. This also indicates that tectonic basins, such as a pull-apart basin, caused by lateral fault motions could not form if the lateral fault has a dip lower than 70°. On the other hand, if the fault dip is higher than 70°, the basement of the footwall side of the lateral fault would begin to subside around the terminus. Additionally, in the case of a fault dip of 90°, uplift of the basement of the hanging wall side would be equal to the subsidence of the basement of the footwall side. This indicates that a fault dip higher than 70° would be required to form tectonic basins due to lateral fault motions. From **Figure 16**, it was found that even if fault scale and lateral motion are the same, the surface deformation patterns would be different as an effect of fault dip. Specifically, surface deformations are basically dependent on fault dip.

6. Discussion

Gravity anomaly analyses, gravity gradient tensor analyses, and seismic surveys are important and useful for finding subsurface structures, and these subsurface structures play an important role for understanding the tectonics and formation processes of the area of concern. In the numerical simulations for restoring the subsurface structures, tectonic topography, and geological structures, we referred often to the subsurface structure given by geophysi-

cal explorations or geological surveys and made basic or initial structure models for the simulations (e.g., [55, 56, 60]).

We paid attention to the contradiction of the MTL being a right-lateral fault in the Quaternary, despite the fact that several seismic surveys have estimated its fault dip to have low angle.

For confirmation, we attempted to extract the MTL trace from the Bouguer anomaly by using several excellent edge emphasis techniques, but high dip-angle traces were not found. In addition, a state-of-the-art dip estimation technique using eigenvector analyses of the gravity gradient tensor could not suggest a high fault dip of the MTL. These facts showed that the MTL does not have a conspicuous density contrast at its motion boundary and that it has low dip as a material boundary.

Considering these results and the actual fault motion of the MTL, we paid attention to the deformation field at the fault terminus having an important role in the formation of tectonic basins caused by lateral fault motions, and we attempted to evaluate the fault dip from the viewpoint of fault motion. As a result, it was found that even if fault scale and lateral motion are the same, the surface deformation patterns at the fault terminus are controlled by fault dip. Specifically, if fault dip is lower than 70°, subsidence areas would not form at the fault terminus, but if fault dip is higher than 70°, both a subsidence area and an uplift area would form at the terminus.

As the present tectonic topography is an accumulation of uplift and subsidence caused by fault motions, we can apply the results shown here to the field as a first approximation without viscoelasticity and plastic flow of the crust at the geological time scale. Consequently, we can roughly estimate the fault dip from the deformed basement and/or sedimentary layer shape.

Conspicuous late Quaternary uplift and subsidence have not been found at the footwall of the MTL because (1) Pliocene layers distribute conspicuously around the eastern portion, the so-called Gojo area, of the footwall of the MTL [61]; (2) there are no new Quaternary layers in boring data obtained around the Kokawa area [8]; and (3) only two marine sediment clay layers of the last interglacial stage (Ma 12: discrimination name in Japan) and alluvium (Ma 13: discrimination name in Japan) in the marine sediment clay layers (Ma 1–13) found in Osaka Bay and Osaka basin have been found in the Wakayama Plain [62]. In addition, trench excavation studies show that the MTL is a vertical or subvertical fault, as was pointed out by Tsutsumi et al. [3], Yamazaki et al. [63], and others. Itoh et al. [12] also found high-dip faults in the Quaternary layer in the seismic profile given by Yoshikawa et al. [5]. Considering these geological and geomorphological evidences and the numerical simulation results of this study, we believe that a fault dip of 70–75° is a reasonable dip angle for the MTL. With a dip of 70–75°, the fault would be able to move as a lateral fault and also have the possibility of reverse-fault motion.

Because the technique of restoring geological structures or topography by numerical simulations is a useful method for evaluating the relationship between fault motions and such structures (e.g., [54–58]), our approach, which is an extension of this technique, should contribute to research of active faults. Although this study employed the dislocation solution in

http://dx.doi.org/10.5772/67964

linear elastic medium as the procedure of numerical simulation, a more detailed and higher accuracy discussion of fault motion and fault shape will be possible by employing a more realistic method such as finite element modeling, discrete element modeling, or other higher techniques (e.g., [64–66]).

On the other hand, new questions that should be discussed and solved in the future were revealed: (1) Why does the motion boundary of the MTL not correspond to the material boundary? (2) How did this structure or contradiction occur? (3) Can the process be explained from the viewpoints of both structural geology and geophysics? (4) Is the process compatible with regional tectonics? (5) Do faults of this type exist in other areas? To discuss and solve these problems, the ideas, suggestions, and interpretations of the tectonics and structures shown by Sato et al. [15] may be useful and helpful, although it is difficult to accept directly lateral fault motion of a low-dip fault. Therefore, we need to continue to study the MTL in the future.

7. Conclusions

Because the MTL is a very important tectonic line for understanding the tectonics in and around southwest Japan, many geological, geophysical, and topographical surveys have been conducted on it. Several reflection surveys have indicated that the MTL has very low dips of less than 55°. As these low-dip faults would not generally move as a lateral fault, the MTL presents a contradiction between its fault dip and fault motion. In addition, because the MTL is proximal to several cities and because fault dip is an important factor for hazard map creation, it is important to estimate the fault dip of the MTL as a seismogenic fault correctly.

In this study, we first attempted to extract the MTL trace and estimate the fault dip from the Bouguer anomaly and gravity gradient tensor, as a confirmation of previous and conventional results. However, these methods could not reveal any high dip-angle faults, because the MTL does not have a conspicuous density contrast at its boundary and has low dip as a material boundary.

To estimate the fault dip of the MTL from the viewpoint of fault motion, we next attempted to evaluate deformation fields at the fault terminus by numerical simulations based on dislocation theory in an elastic medium. The result showed that the surface deformation patterns at the fault terminus are controlled by fault dip if fault scale and lateral motion are the same. If the fault dip was lower than 70°, subsidence areas did not form at the fault termination. However, if the fault dip was higher than 70°, both subsidence and uplift areas formed at the terminus. Considering the accumulated geological and geomorphological evidence for the motion of the MTL in the Quaternary, and our numerical simulation results, we suggest that a fault dip of 70–75°, at which the fault would be able to move as a lateral fault with a reverse-fault component, is a reasonable value for the fault dip of the MTL (as a seismogenic fault).

Our results and suggestions indicate that the motion boundary of the fault does not correspond with the material boundary. In the future, it will be important to research this formation mechanism, including whether or not this type of fault exists in other areas.

Acknowledgements

This study was executed as a part of the Comprehensive Research and Survey for the Median Tectonic Line Fault System (Eastern Margin of Kongo Mountains-Southern Margin of Izumi Mountains; FY 2013-2015) organized by the Research and Development Bureau, MEXT, and the DPRI, Kyoto University. This work was supported partially by Japan Society for the Promotion of Science (JSPS) KAKENHI Grant Number 15K14274. The authors are grateful to the agency. And, the authors are also most grateful to Yoichi Fukuda for very useful comments that have considerably improved the manuscript. In addition, the authors are most grateful to Ana Pantar for her editorial advices and cooperation.

Author details

Shigekazu Kusumoto[1]*, Keiji Takemura[2] and Yasuto Itoh[3]

*Address all correspondence to: kusu@sci.u-toyama.ac.jp

1 Graduate School of Science and Technology for Research, University of Toyama, Toyama, Japan

2 Kyoto University, Sakyo-ku, Kyoto, Japan

3 Osaka Prefecture University, Sakai, Osaka, Japan

References

[1] Fitch T J. Plate convergence, transcurrent faults, and internal deformation adjacent to southeast Asia and the western Pacific. Journal of Geophysical Research 1972; **101**: 4432-4460.

[2] McCaffrey R. Slip partitioning at convergent plate boundaries of SE Asia. Geological Society of London Special Publication 1996; **106**: 3-18.

[3] Tsutsumi H, Okada A, Nakata T, Ando M, Tsukuda T. Timing and displacement of Holocene faulting on the Median Tectonic Line in central Shikoku, SW Japan. Journal of Structural Geology 1991; **13**: 227-233.

[4] Tsutsumi H, Okada A. Segmentation and Holocene surface faulting on the Median Tectonic Line, southwest Japan. Journal of Geophysical Research 1996; **101**: 5855-5871.

[5] Yoshikawa S, Iwasaki Y, Ikawa T, Yokota H. Geological structure of the MTL in west Wakayama by reflection seismic survey. Memories of the Geological Society of Japan 1992; **40**: 177-186 (in Japanese with English abstract).

[6] Yusa Y, Takemura K, Kitaoka K, Kamiyama K, Horie S, Nakagawa I, Kobayashi Y, Kubotera A, Sudo Y, Ikawa T, Asada M. Subsurface structure of Beppu Bay (Kyushu,

Japan) by seismic reflection and gravity survey. Zisin 2nd series 1992; **45**: 199-212 (in Japanese with English abstract).

[7] Ito T, Ikawa T, Yamakita S, Maeda T. Gently north-dipping Median Tectonic Line (MTL) revealed by recent seismic studies, southwest Japan. Tectonophysics 1996; **264**: 51-63.

[8] Mizuno K, Tsukuda E, Takahashi M, Momohara A, Uchiyama T. Subsurface geology of the Wakayama Plain, southwestern Japan based on the deep boring survey. Journal of Geological Society of Japan 1999; **105**: 235-238 (in Japanese with English abstract).

[9] Kawamura T, Onishi M, Kurashino E, Ikawa T, Ito T. Deep seismic reflection experiment using a dense receiver and sparse shot technique for imaging the deep structure of the Median Tectonic Line (MTL) in east Shikoku, Japan. Earth Planets Space 2003; **55**: 549-557.

[10] Ito T, Kojima Y, Kodaira S, Sato H, Kaneda Y, Iwasaki T, Kurashimo E, Tsumura N, Fujiwara A, Miyauchi T, Hirata N, Harder S, Miller K, Murata A, Yamakita S, Onishi M, Abe S, Sato T, Ikawa T. Crustal structure of southwest Japan, revealed by the integrated seismic experiment Southwest Japan 2002. Tectonophysics 2009; **472**: 124-134.

[11] Shigematsu N, Fujimoto K, Tanaka N, Furuya N, Mori H, Wallis S. Internal structure of the Median Tectonic Line fault zone, SW Japan, revealed by borehole analysis. Tectonophysics 2012; **532-535**: 103-118.

[12] Itoh Y, Takemura K, Kusumoto S. Neotectonic intra-arc basins within southwest Japan — Conspicuous basin-forming process related to differential motion of crustal blocks. In: Itoh Y. (ed.) Mechanism of Sedimentary Basin Formation: Multidisciplinary Approach on Active Plate Margins. Rijeka: InTech; 2013, pp. 191-206.

[13] Anderson E M. The Dynamics of Faulting and Dyke Formation with Applications to Britain. 2nd edition. Edinburgh: Oliver and Boyd; 1951. 206 p.

[14] Turcotte D, Schubert G. Geodynamics. 2nd edition. Cambridge: Cambridge University Press; 2002. 456 p.

[15] Sato H, Kato N, Abe S, Horne A V, Takeda T. Reactivation of an old plate interface as a strike-slip fault in a slip-partitioned system: Median Tectonic Line, SW Japan. Tectonophysics 2015; **644-645**: 58-67.

[16] Abrahamson N A, Somerville P. Effects of the hanging wall and footwall on ground motions recorded during the Northridge earthquake. Bulletin of Seismological Society of America 1996; **86**: S93-S99.

[17] Takemura M, Moroi T, Yashiro K. Characteristics of strong ground motions as deduced from spatial distributions of damages due to the destructive inland earthquakes from 1891 to 1995 in Japan. Zisin 2 1998; **50**: 485-505 (in Japanese with English abstract).

[18] Irikura K, Miyake H. Recipe for predicting strong ground motion from crustal earthquake scenarios. Pure and Applied Geophysics 2011; **168**: 85-104. doi 10.1007/s00024-010-0150-9.

[19] Komazawa M. Gravity grid database of Japan. DVD Edition, Digital Geoscience Map P-2. Tsukuba: Geological Survey of Japan, AIST. 2013.

[20] Blakely R, Simpson R W. Approximating edges of source bodies from magnetic or gravity anomalies. Geophysics 1986; **51**: 1494-1498.

[21] ten Brink, U S, Ben-Avarham Z, Bell R E, Hassouneh M, Coleman D F, Andreasen F, Tibor G, Coakley B. Structure of the Dead Sea Pull-apart Basin from Gravity Analyses. Journal of Geophysical Research 1993; **98**: 21877-21894.

[22] Shichi R, Yamamoto A, Kimura A, Aoki H. Gravimetric evidences for active faults around Mt. Ontake, central Japan: specifically for the hidden faulting of the 1984 Western Nagano Prefecture Earthquake. Journal of Physics of the Earth 1992; **40**: 459-478.

[23] Kudo T, Kono Y. Relationship between distributions of shallow earthquakes and gradient of gravity anomaly field in southwest Japan. Zishin 2 1999; **52**: 341-350 (in Japanese with English abstract).

[24] Yamamoto A. Gravity anomaly atlas of the Ishikari Plain and its vicinity, Hokkaido, Japan. Geophysical Bulletin of Hokkaido 2003; **66**: 33-62 (in Japanese with English abstract).

[25] Li L, Huang D, Han L, Ma G. Optimized detection filters in the interpretation of potential field data. Exploration Geophysics 2014; **45**: 171-176. doi: 10.1071/EG13059.

[26] Zhang X, Yu P, Tang R, Xiang Y, Zhao C-J. Edge enhancement of potential field data using an enhanced tilt angle. Exploration Geophysics 2014; **46**: 276-283. doi:10.1071/EG13104.

[27] Miller H G, Singh V. Potential field tilt—a new concept for location of potential field sources. Journal of Applied Geophysics 1994; **32**: 213-217.

[28] Wijns C, Perez C, Kowalezyk P. Theta map: edge detection in magnetic data. Geophysics 2005; **70**: L39-L43.

[29] Cooper G R J, Cowan D R. Enhancing potential field data using filters based on the local phase. Computers and Geosciences 2006; **32**: 1585-1591.

[30] Ma G. Edge detection of potential field data using improved local phase filter. Exploration Geophysics 2013; **44**: 36-41.

[31] Ferreira F J F, de Souza J, de B e S Bongiolo A, de Castro L G. Enhancement of the total horizontal gradient of magnetic anomalies using the tilt angle. Geophysics 2013; **78**: J33-J41.

[32] MEXT (Ministry of Education, Culture, Sports, Science and Technology, Japan), DPRI (Disaster Prevention Research Institute, Kyoto University). Comprehensive Research and Survey for the Median Tectonic Line Fault System (Eastern Margin of Kongo Mountains—Southern Margin of Izumi Mountains), Heisei 25 Fiscal Year Report. Uji: DPRI; 2014.

[33] Kusumoto S, Fukuda Y, Takemoto S, Yusa Y. Three-dimensional subsurface structure in the eastern part of the Beppu-Shimabara Graben, Kyushu, Japan, as revealed by Gravimetric Data. Journal of the Geodetic Society of Japan 1996; **42**: 167-181.

[34] Talwani M, Lamar W J, Landisman M. Rapid gravity computations for two-dimensional bodies with application to the Mendocino submarine fracture zone. Journal of Geophysical Research 1959; **64**: 49-59.

[35] Torge W. Gravimetry. Berlin: Walter de Gruyter; 1989. 465 p.

[36] Hofmann-wellenhof B, Moritz H. Physical Geodesy. Berlin: Springer; 2005. 403 p.

[37] Zhang C, Mushayandebvu M F, Reid A B, Fairhead J D, Odegrad M E. Euler deconvolution of gravity tensor gradient data. Geophysics 2000; **65**: 512-520.

[38] Beiki M, Pedersen L B. Window constrained inversion of gravity gradient tensor data using dike and contact models. Geophysics 2011; **76**: I59-I70.

[39] Martinetz C, Li Y, Krahenbuhl R, Braga M A. 3D inversion of airborne gravity gradiometry data in mineral exploration: a case study in the Quadrilatero Ferrifero, Brazil. Geophysics 2013; **78**: B1-B11.

[40] Cevallos C. Automatic generation of 3D geophysical models using curvatures derived from airborne gravity gradient data. Geophysics 2014; **79**: G49-G58.

[41] Li X. Curvature of a geometric surface and curvature of gravity and magnetic anomalies. Geophysics 2015; **80**: G15-G26.

[42] Beiki M, Pedersen L B. Eigenvector analysis of gravity gradient tensor to locate geologic bodies. Geophysics 2010; **75**: I37-I49.

[43] Kusumoto S. Dip distribution of Oita-Kumamoto Tectonic Line located in central Kyushu, Japan, estimated by eigenvectors of gravity gradient tensor. Earth Plan Space 2016; **68**: 153. doi: 10.1186/s40623-016-0529-7.

[44] Beiki M. TSVD analysis of Euler deconvolution to improve estimating magnetic source parameters: an example from the Asele area, Sweden. Journal of Applied Geophysics 2013; **90**: 82-91.

[45] Kusumoto S. Estimation of dip angle of fault or structural boundary by eigenvectors of gravity gradient tensors. Butsuri-Tansa 2015; **68**: 277-287 (in Japanese with English abstract).

[46] Kusumoto S. Eigenvector of gravity gradient tensor for estimating fault dips considering fault type, Progress in Earth and Planetary Science. 2017.

[47] Mickus K L, Hinojosa J H. The complete gravity gradient tensor derived from the vertical component of gravity: a Fourier transform technique. Journal of Applied Geophysics 2001; **46**: 159-174. (Accepted with minor revision).

[48] Miura S, Ueki S, Sato T, Tachibana K, Hamaguchi H. Crustal deformation associated with the 1998 seismo-volcanic crisis of Iwate volcano, northeastern Japan, as observed by a dense GPS network. Earth Planets Space 2000; **52**: 1003-1008.

[49] Owen S, Segall P, Lisowski M, Murray M, Bevis M, Foster J. The January 30, 1997, eruptive event on Kilauea volcano, as monitored continuous GPS. Geophysical Research Letters 2000; **27**: 2757-2760.

[50] Fialko Y, Simons M, Agnew D C. The complete (3-D) surface displacement field in the epicentral area of the 1999 Mw 7.1 Hector mine earthquake, California, from space geodetic observations. Geophysical Research Letters 2001; **28**: 3063-3066.

[51] Jonsson K M, Hsu Y J, Segall P, Yu S B. Fault geometry and slip distribution of the 1999 Chi-Chi, Taiwan, earthquake imaged from inversion of GPS data. Geophysical Research Letters 2001; **28**: 2285-2288.

[52] Lasserre C, Peltzer G, Crampe F, Klinger Y, Van der Woerd J, Tapponnier P. Coseismic deformation of the 2001 Mw=7.8 Kokoxili earthquake in Tibet, measured by synthetic aperture radar interferometry. Journal of Geophysical Research 2005; **110**: doi: 10.1029/2004JB003500.

[53] Okada Y. Surface deformation due to shear and tensile faults in a half-space. Bulletin of Seismological Society of America 1985; **75**: 1135-1154.

[54] Rodgers D A. Analysis of pull-apart basin development produced by en echelon strike-slip faults. Special Publications, International Association of Sedimentologists 1980; **4**: 27-41.

[55] Katzman R, ten Brink U S, Lin J. Three-dimensional modeling of pull-apart basins: Implications for the tectonics of the Dead Sea Basin. Journal of Geophysical Research 1995; **100**: 6295-6312.

[56] Kusumoto S, Takemura K, Fukuda Y, Takemoto S. Restoration of the depression structure at the eastern part of central Kyushu, Japan, by means of the dislocation modeling. Tectonophysics 1999; **302**: 287-296.

[57] Itoh Y, Kusumoto S, Furubayashi T. Quantitative evaluation of the Quaternary crustal deformation around the Takayama basin, central Japan: A paleomagnetic and numerical modeling approach. Earth and Planetary Science Letters 2008; **267**: 517-532. doi: 10.1016/j.epsl.2007.11.062.

[58] Tamaki M, Kusumoto S, Itoh Y. Formation and deformation process of the late Paleogene sedimentary basins in the southern central Hokkaido, Japan: paleomagnetic and numerical modeling approach. Islands Arc 2010; **19**: 243-258.

[59] Kusumoto S, Itoh Y, Takano O, Tamaki M. Numerical Modeling of Sedimentary Basin Formation at the Termination of Lateral Faults in a Tectonic Region where Fault Propagation has Occurred. In: Itoh, Y. (ed.), Mechanism of sedimentary basin formation: multidisciplinary approach on active plate margins. Rijeka: InTech; 2013, pp. 273-303.

[60] Itoh Y, Takano O, Kusumoto S, Tamaki M. Mechanism of longstanding Cenozoic basin formation in central Hokkaido: an integrated basin study on an oblique convergent margin. Progress in Earth and Planetary Science 2014; **1**: 6. doi: 10.1186/2197-4284-1-6.

[61] Mizuno K, Momohara A. Shobudani Formation, terrace and alluvial In: Ichihara, M. (ed.), Osaka Group. Osaka: Sohgen-sya; 1993, pp. 145-157

[62] KG-net and Kansai Geo-informatics Research Committee, Shin-Kansai geo-informatics—Wakayama Plain. Yodogawa-kohgi, Osaka, 2011.

[63] Yamazaki H, Tsukuda E, Okumura K, Kinugasa Y, Okada A, Nakata T, Tsutsumi H, Hasegawa S. Trench excavation of the Okamura fault in the Median Tectonic Line fault system at Saijo, southwest Japan. Memories of the Geological Society of Japan 1992; **40**: 129-142 (in Japanese with English abstract).

[64] Cundall P A, Strack O D L. A discrete numerical model for granular assemblies, Géotechnique 1979; **29**: 47-65.

[65] Hardy S, McClayc K, Muñoz J A. Deformation and fault activity in space and time in high-resolution numerical models of doubly vergent thrust wedges. Marine and Petroleum Geology 2009; **26**: 232-248.

[66] Kusumoto S, Itoh Y, Takemura K, Iwata T. Displacement fields of sedimentary layers controlled by fault parameters: the discrete element method of controlling basement motions by dislocation solutions. Earth Sciences 2015; **4**: 89-94.

[67] Hayama Y, Yamada T. Median Tectonic Line at the stage of its origin in relation to Plutonism and Mylonitization in the Ryoke belt. Memories of the Geological Society of Japan 1980; **18**: 5-26.

[68] Geological Survey of Japan, AIST (ed.). Seamless digital geological map of Japan 1: 200,000. May 29, 2015 version. Geological Survey of Japan, National Institute of Advanced Industrial Science and Technology, Tsukuba.

INTECH